IOP Conf. Series: Materials Science and Engineering **413** (2018) 012035 doi:10.1088/1757-899X/413/1/012035

Evaluation of Friction Stir Welds by X-ray Digital Radiographic Non- Destructive Approach

Itai Mumvenge[1, a], Stephen A. Akinlabi[2, b], Peter M. Mashinini[2, c] Olawale S. Fatoba[1d], Joshua Okeniyi[1e,3f], and Esther T. Akinlabi[1g]

[1]Department of Mechanical Engineering Sciences, University of Johannesburg, South Africa, [2] Department of Mechanical and Industrial Engineering Technology, University of Johannesburg, South Africa, [3]Department of Mechanical Engineering, Covenant University, Ota, Nigeria.
Email: [a]itaimumvenge@gmail.com, [b]stephenakinlabi@gmail.com, [c]mmashinini@uj.ac.za, [d]drfatobasameni@gmail.com, [e]jokeniyi@uj.ac.za, [f]joshua.okeniyi@covenantuniversity.edu.ng, [g]etakinlabi@uj.ac.za

Abstract. This paper focuses on the microstructure evolution and the relationship to the microhardness profiling of the friction stir welded butt joint on similar AA6061-T6 Aluminium alloys. The only parameters used and varied for this study were rotational speed and feed rate. The geometry of the tool was kept constant and the material used was tool steel, W302. Friction stir welds were evaluated by both visual inspection and the X-ray digital radiography method. Evaluation allowed for assessment of the weld integrity by examining for the presence and absence of weld defects. The results indicated that the welds do not have any root defects. The X-rays showed complete penetration as evidenced by the evaluation of microstructural joint interface.

1. Introduction

Friction stir welding is a novel solid-state welding technique that was invented at The Welding Institute (TWI) of UK in 1991 by Wayne Thomas [1], and was initially applied to aluminium alloys [2]. The welds are made by plunging a rotating non-consumable Friction Stir Welding (FSW) tool pin on the abutting edges of a work-piece where the rotational speed causes friction to generate localized heat energy to achieve plastic deformation of the work-piece material. As the FSW tool traverses, the frictional heat also traverses along the joint-line [3].

Like any new technology, material flow complexities and weld processes and application can result in weld flaws. In the case of FSW, inappropriate processing conditions can cause formation of various visible or potential defects around the weld nugget zone (WNZ), the thermo-mechanically affected zone (TMAZ), or sometimes at the WNZ/TMAZ interface [4]. This results in FSW weld-defect of different types, which includes voids, defective tightness, surface groove, excessive flash, 'kissing-bond' [5] and crack-like root-flaws, which are quite different from conventional fusion welding flaws [6].

Defects are inherent to most joint during welding processes [7]. The formation of weld defects within the friction stir welds is mainly caused by inappropriate FSW process parameters. Some of these process parameters that may contribute to the formation of weld defects are mostly tool rotational speed [8], travel speed, tilt angle, shoulder target depth [9], applied load and pin configuration [10].

With recent developments in technology, weld integrity can be evaluated without physical destruction of the weld by non-destructive approach. Non-destructive testing (NDT) relies on the use of physics principles such as acoustic waves and radiation, to ascertain the physical appearance of materials, detecting material flaws and critical defects [11]. The important characteristics of non-destructive testing is the ability to evaluate material and weld flaws without altering the serviceability or effectiveness of the said components, on the other word, it does not damage the material. NDT has vast benefits, some of which include cost effectiveness, great reliability and safer applicability for a wide range of processes.

Commercial use of NDT is widely spread in industrial fields, especially on railway, petrochemical pressure tanks, power generation, aviation, automotive and mining infrastructure inspections [12]. On the contrary, the weld bending test and the micro-optical observation by bending weld samples will both make the materials ineffectual, and they only give understanding into the weld features at the damaged point where the rupture or the material appearance information is acquired, the better option is thus non-destructive testing [13].

Radiographic testing (RT) is one typical non-destructive testing technique used to analyze hidden flaws by using short wavelength electromagnetic radiation to penetrate materials. A radioactive source uses photons such as Ir-192, Co-60 and Cs-137. Neutrons can also be used as a replacement for photons to penetrate the material. X-ray radiography can also be used to analyze weld defects [14]. Digital image processing is carried out on a local or neighbor-hood operation point using several pixels in a limited area of the input image to obtain a point in the processed or final image" [15].

Gaurav *et al*., [15], performed a digital radiography test for Gas Tungsten Arc Welding (GTAW) and FSW weldments of AA7075-T651 aluminum alloy and they observed the defect of porosity, cluster porosity and small tunnel defect. Edwards et al., [16], used X-ray radiography and validated with metallographic images to examine friction stir welded 6mm thick Ti-6Al-4V butt joints processed and embedded with a tracer material. A variety of rotational and traverse speeds were implemented. The conclusion was that X-ray radiography scans could depict the characterization of the material flow behavior [16].

Patil *et al*., [17], applied X-ray radiography testing technique to analyze weld defects in similar and dissimilar friction stir welded aluminum alloy butt weld joints. The material used was AA7075 T651 in butt weld joint configuration for similar welds. Dissimilar weld joints were processed using aluminum alloys AA77075 T651 and AA6061 T6. Different tool rotational speeds (800, 900, 1000 rpm) and feed rates (30, 35, 40mm/min) were employed while all the other process parameters were kept constant. The visual inspection was only able to identify flash formation on all the samples. The X-ray radiographic testing techniques revealed a lack of penetration in all weld samples such as cracks, voids and wormhole defects. It was concluded that the X-ray radiography was successful in evaluating the weld defects of the friction stir weld sample for similar and dissimilar materials. It was also observed that increasing the transverse speed, increases the occurrence of weld defects [17].

Some of the weld defects can be difficult to detect using visual inspection techniques or certain types of non-destructive evaluation techniques. It is therefore imperative that the correct selection of inspection method and its parameters are well defined to effectively evaluate the microstructure, defects and the integrity of the friction stir weld. This research work focuses and reports on the non-destructive testing to identify the root defect in friction stir welded joints as applied to AA6061-T6 Aluminium alloys.

2. Experimental Set-Up

The friction stir weld process was conducted using a computer controlled 2-Axis FSW machine at the Indian Institute of Science (IISC), Bangalore, India. The parent material used in this study was an AA6061-T6 aluminum alloy with dimensions measuring 200 x 150 x 4.09 mm3 and having a friction stir welded butt joint length of 120mm. The predominantly concave shoulder with a pin attachment provides confinement for the heated volume of the material.

A spectrometer was used to analyze the chemical composition of the parent material, which was found to be in accordance with the AA6061-T6 standard specifications [21]. The chemical composition of the welded material is shown in Table 1.

Table 1 Chemical Composition of Aluminium AA6061-T6

Element	Si	Fe	Cu	Mn	Mg	Cr	Ni	Zn	Ti	Al	Ag
Wt %	0.68	0.49	0.21	0.08	0.84	0.06	0.01	0.07	0.07	97.40	Balance

A concave tool shoulder with a threaded pin length of 3.8mm was produced from tool steel W302 and used to produce the welds. A weld matrix with criteria category of low, medium and high settings was used to define the combinations of rotational and feed rates. Table 2 shows the optimum process parameters matrix developed for the friction stir welded samples. The pin movement and geometry stir the material, facilitated the downward mixing auger effect [18]. The FSW schematic is illustrated in Figure 1. The fine microstructure generated helped achieve mechanical properties of sufficiently high strength, fatigue and fracture resistant welds [19].

Table 2. Process Parameter Matrix of the FSW process

Weld Designation	Rotational Speed (rpm)	Feed Rate (mm/min)	Code
BW1	700	60	Ll
BW2	700	80	Lm
BW3	700	100	Lh
BW4	900	60	Ml
BW5	900	80	Mm
BW6	900	100	Mh
BW7	1100	60	Hl
BW8	1100	80	Hm
BW9	1100	100	Hh

L = low rotation speed, l = low feed rate
M= Medium rotational speed, m = medium feed rate
H= High rotational speed, h = high feed rate

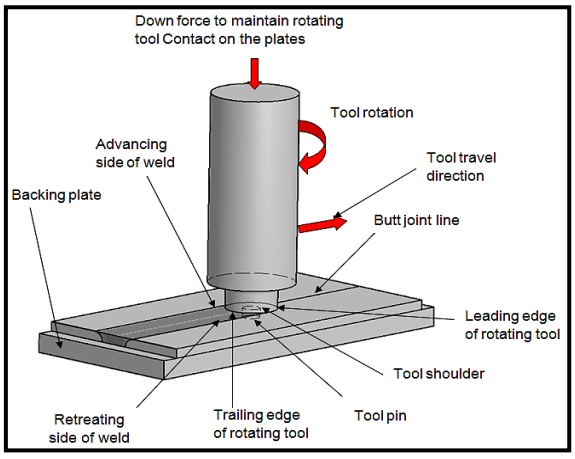

Fig. 1 Schematic of a FSW tool movements on a workpiece **[20]**

Samples were cut and sectioned from the weld coupons. These samples were etched using Weck's reagent. Microstructure observations were conducted using the Olympus BX51M and macrographs for the welds were taken using the Olympus SZX16.

Vickers microhardness were measured using a TH713 Vickers microhardness tester, by Beijing Cap High Technology Co. Ltd in accordance to ASTM 384-16 [22]. Tensile testing was also conducted. The tensile samples specification dimensions were in accordance to the ASTM B557-14 standard [23] while the tensile testing procedure was conducted in accordance to the ASTM E8M-13 standard [24].

The visual inspections on the welds were conducted and the X-ray digital radiography was performed on the test samples to inspect weld defects using the equipment Vidico fox-Raysor, 80kV, 0.6A and Balteau X-ray source. The radiography procedure was conducted according to the ASTM E155-15 standard specification [25]. The foX-Rayzor FPD was used in combination with a Vidisco supplied 270 kV pulsed x-ray source or almost any X-ray source / isotope. The recommended X-ray sources must be up to 160 kV, otherwise shielding is required for higher voltages. Table 3 shows the exposure parameters that were used to produce the X-ray radiographs scan images.

Table 3 X-ray Radiography Exposure Parameters for FSW joints

Process Parameter	Value
Electrical Voltage Range	700
Tube Current Range	700
Exposure Time	700
X-ray tube beam angle	900
Focal spot size	900
X-ray inherent filtration mm	900
Source to Object Distance (SOD)	1100

3. Results and Discussion

3.1. Weld Defects Analysis

Table 4 shows the physical appearances and X-ray scans of the friction stir processed weld joints with the aim of showing defects caused by the generation of high temperature combined with severe local shearing action due to the tool movement. The curling wavelike flashes are a result of the movement of plasticized material displaced by the pin with the tool shoulder not confining the material. The tool rotational speed of 700 rpm and 100 mm/min appear to have processed a weld with the least flash sizes.

It was demonstrated from the results that weld flash is necessitated by material flow behavior which is predominantly influenced by the FSW process parameters such as the tool rotational speed. It is noticeable, that rotational speed appears to be the predominant influencing process variable since it is associated with the translational velocity. Murr, *et al.,* [7], reported that an increase in strain rate can influence the re-crystallization process and these strain rates are associated with very high rotational speeds, which influence the generation of excessively large weld flash [7]. Also, low heat inputs are predominantly associated with higher welding speeds which causes the welded joint to be cooled at a faster rate. The curled flash could thus be attributed to incorrect combinations of the rotational speed and the feed rate which in instances yields low axial forces. Such low axial forces, contribute to the formation of non-symmetrical semi-circular features and in instances, large flash at the top surface of the weld due to poor plasticization and consolidation of the material under the influence of the tool shoulder [9]. The non-symmetrical semi-circular features were not evident with the visual inspection on

all the welds. This implies that the welds were homogenous and of sound quality. This inspection needed to be verified by an optical microscopy and other analytical techniques.

Table 4 contains the X-ray radiograph scan images and the respective comments on each examined sample. All the friction stir welds were observed to be defect free from voids and porosity, which could be attributed to good material flow ability due to optimal heat energy. A keyhole was observed in the workpiece at the pin's point of retraction which is a known phenomenon in FSW. Research literature shows that an exit hole can be repaired by eliminated by active passing filling friction stir repair [21, 22].

Table 4 Physical Appearance of the FSW samples

Rotational Speed (rpm)	60mm/min		80mm/min		100mm/min		Comments
	photo	X-ray Image	photo	X-ray Image	photo	X-ray Image	
700							No evidence of root defects was observed on all the welds produced using the 700-rpm rotation speed and the respective feed rates. Keyhole observed.
900							No evidence of root defects was observed on all the welds produced using the 900-rpm rotation speed with the 60 and 80 mm/min feed rates. An insignificant root defect can be seen for the weld produced with the feed rate of 100 mm/min. Keyhole observed.
1100							No evidence of root defects was observed on all the welds produced using the 1100 rpm rotation speed and the respective feed rate speeds. Keyhole observed.

3.2. Macrostructure and Microstructure Analysis

Figure 2 shows the typical macrograph of the friction stir welded sample produced at 700 rpm and feed rate of 80 mm/min. All the macrographs showed no internal defect present in any of the weld samples done for this research work. The morphological features noticed using the optical microscope consisted of all the four distinct FSW microstructural zones namely: TMAZ, HAZ and SZ or NZ, and the Parent material.

An optical microscopy examination was used to identify the FSW microstructural zones of all the welds produced. Figure 3 shows the typical microstructures on the different zones obtained in the weld's stabilized region. From observation, the evolution of the morphology from the base metal is quite remarkable.

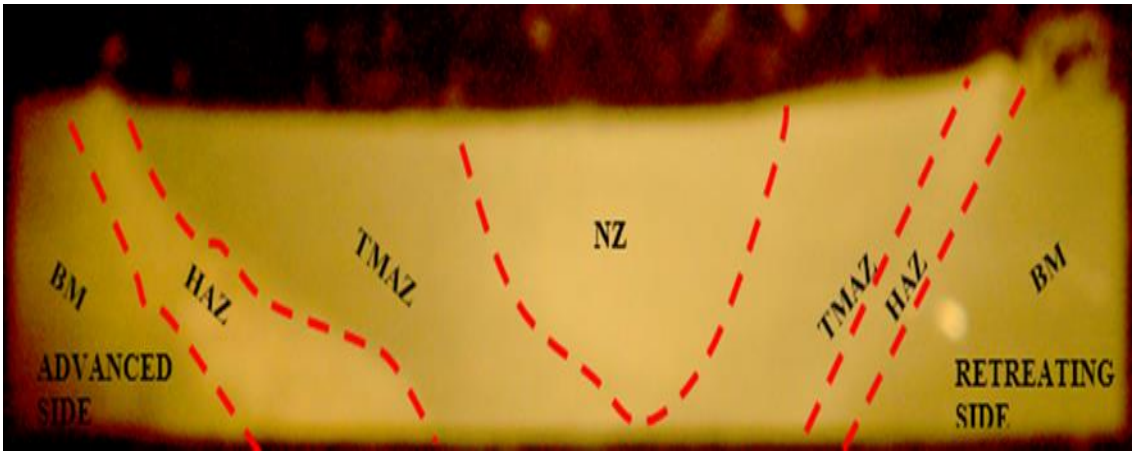

Fig. 2 Typical Macrograph of FSW butt joint produced at weld speeds 700 rpm and 80 mm/min

Optical microscopy and Scanning Electron Microscopy (SEM) examinations were used to study the FSW microstructure zones for all the welds produced. Figure 3 (a) showed a base metal microstructure with a honeycomb-like shape, also revealed in the SEM micrograph presented in Figure 3(b). The presence of the second phase precipitates can be seen in the microstructure analyzed using SEM. These precipitates are mostly elements of Mg2Si [12]. Figure 4 presents the microstructural evolution of the weld sample produced at 700rpm and 80mm/min. The weld zones' diffuse contrast can be observed indicating the different material thermo-flow and stresses [23] not analyzed in this study.

Optical microscopy and Scanning Electron Microscopy (SEM) examinations were used to study the FSW microstructure zones for all the welds produced. Figure 3 (a) shows the base metal microstructure with a honeycomb-like shape as revealed in the SEM micrograph presented in Figure 3(b). The presence of the second phase precipitates can be seen in the microstructure analyzed using SEM. These precipitates are mostly elements of Mg2Si [12]. Figure 4 presents the microstructural evolution of the weld sample produced at 700rpm and 80mm/min. The weld zones' diffuse contrast can be observed indicating the different material thermo-flow and stresses [23] not analyzed in this study.

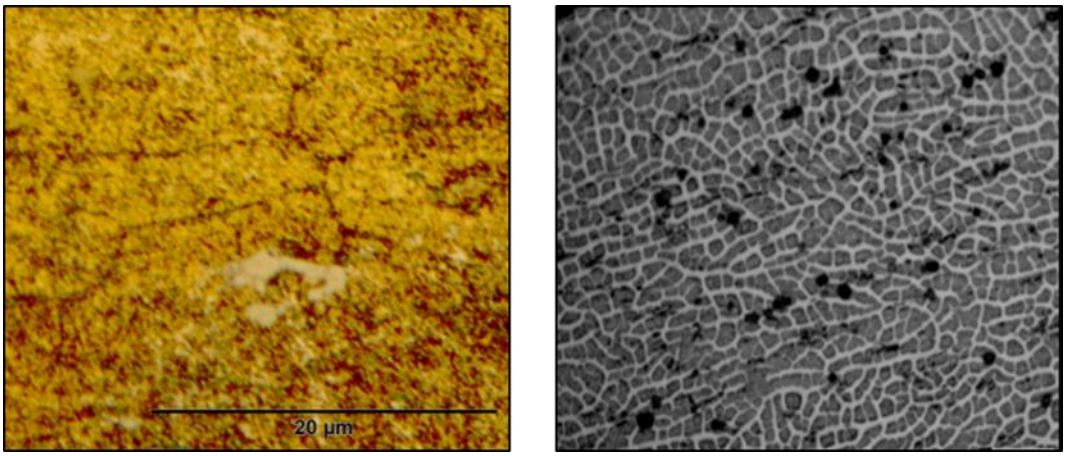

Fig. 3 AA6061-T6 Base Metal Microstructure (a) OM micrograph (b) SEM

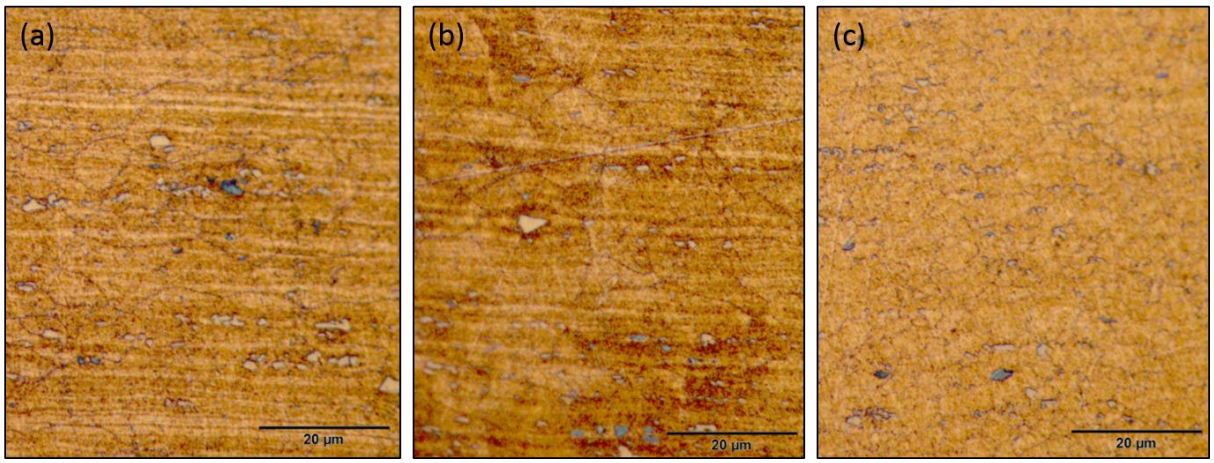

Fig. 4 Typical Microstructure micrographs of the (a) BM (b) HAZ (c) TMAZ (d) WN produced at weld speeds 700 rpm and 80 mm/min

SEM was used to analyze the weld zone microstructure and the presence of intermetallic particles. The resultant micrographs are shown in Figure 5. All the micrographs have white and grey spots which are evident within the grains. These spots represent intermetallic particle constituents. Weck's reagent can be seen to have attacked some of the intermetallic particles and the grains during the etching process. These attacks should not be confused with the weld defects such as voids, whose absence has already been concluded using non-destructive X-ray testing.

The HAZ (Figure 5(a)), which is common to all welding processes subjected to thermal cycle with no deformation, has slight changes from the base metal. The TMAZ (Figure 5b) grain structure was characterized with mixed rotated, elongated and equiaxed grains which reflects grains of partially recrystallized morphology. The WN (Figure 5(c)), has much smaller fine equiaxed grains due to dynamic recrystallization. Although the micrographs for the retreating side are not presented with this paper, a sharp transition was seen between the TMAZ and the SZ on the advancing side while a much more diffuse interface was observed at the RS. This contrast is in relation to the different material flow conditions on the two sides.

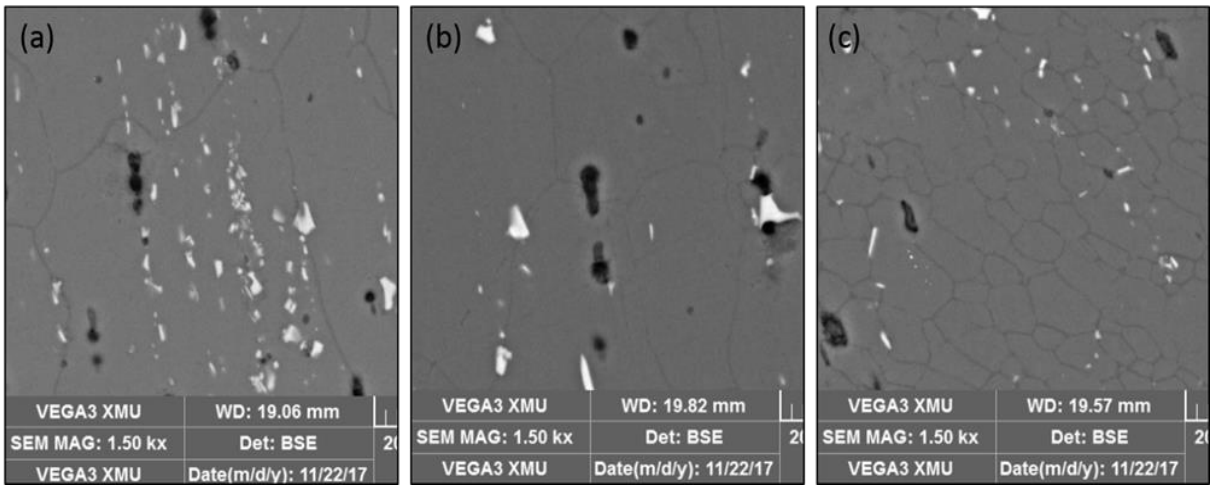

Fig. 5 Typical SEM images of the (a) HAZ (b) TMAZ (c) WN produced at weld speeds 700 rpm and 80 mm/min

As presented in Table 5 below, in the HAZ, exhibiting similar trend to the NZ and TMAZ, the average grain sizes decreased with every increase in the welding speed though it was minimal. For instance, at rotational speed of 700 rpm, the average grain size in the HAZ decreased from 129 µm to 127 µm and

finally 126 μm in correspondence with the increase of welding speed from 60 mm/min, 80 mm/min and 100 mm/min respectively. These results further confirm the findings by Fadaeifard *et al*., [23], in which it was report the grain size decreased with the increase in weld speeds. The increase in deformation rate caused by the rotating tool plays a major role in reducing grain size. However, it is important to note that both frictional heat and deformation rate reduce with the increase in traverse speed [28].

Table 5 Average grain size in various regions

Weld Designation	Rotational Speed (rpm)	Feed Rate (mm/min)	NZ μm	TMAZ μm	HAZ μm	BM μm
BW1	700	60	4.4	85.4	129	125
BW2	700	80	3.7	83.1	127	125
BW3	700	100	3.43	79.2	126	125
BW4	900	60	7.4	92.7	122	125
BW5	900	80	6.8	95.1	121	125
BW6	900	100	5.43	80.2	118	125
BW7	1100	60	14	95.3	133	125
BW8	1100	80	10.1	95.1	128	125
BW9	1100	100	8.7	80.2	125	125

In most of these weld samples, the HAZ grain size is slightly larger than in the base metal (BM). This grain growth is highly influenced by heat input in the weldment. Unlike the rotational speed, the weld traverse speed shows a reverse effect on the heat generated during FSW [24], as such the heat energy reduction is relative to the increase in traverse rate. Previous studies have shown that the stirred zone experiences lower temperatures. A short duration is therefore available for grain growth accompanied with recrystallization effects, which cause smaller grain size in the WN.

Akinlabi *et al*., [25], reported that there is a derived condition that changes the grain size necessitated by a competition between frictional heat and deformation rate at each welding condition such that the grain size is a net effect of deformation rate and frictional effect [31. In this study, it was deduced that the lower welding speeds were effective in increasing the deformation rate and frictional heat resulting in reduced grain size. However, the reduction of grain sizes with increase in welding speeds suggests that frictional heat is dominant than the deformation rate. The increase in weld speeds also necessitated the reduction in peak temperatures and faster cooling rates which assisted in effecting the reduced grain sizes. It is therefore imperative to conclude that the welding parameters such as rotational and traverse speeds play a crucial role in reduced grain sizes.

In Figure 3 (b), small rod/needle-like shaped β" precipitates were observed in the base metal microstructure. The dissolution of these precipitates in the weld samples during FSW can be attributed to the feed rate and the tool rotational speed, which are some of the key parameters, as they respectively influence the heating time and the peak temperature. As such dynamic recrystallization occurs due to intense plastic flow at high temperatures, more so, in the weld nugget to give smaller grain size as recorded in Table 5 and demonstrated in the SEM results in Figure 5(c). The precipitates, which are known to have intense interactions with dislocations and grain boundaries, may start to have effect on dislocation density (driving force) and the recrystallization kinetics. This leads to a microstructural evolution that results in dissolution of precipitates. The smaller grain size in the weld nugget can also be attributed to grain recrystallization because of the pinning effect of these particles. The β'' precipitates are obviously dissolved in the nugget which gave rise to some supersaturated solution in the stirred zone. These heterogeneously distributed precipitates observed in weld nugget gives rise precipitates hardening. The next section will discuss the hardness distribution across the weld traverse

which will be seen to be high in the weld nugget when compared to the TMAZ and HAZ. Sauvage *et al.*, [26] contributed that "two mechanisms exist that lead to the formation of heterogeneously distributed precipitates in the weld nugget". The first consideration is the heterogeneous precipitation due to the great increase of the temperature causing the β'' precipitates dissolve. This was explained to be experienced when the FSW pin is moved away, which drops the temperature and increases the driving force for precipitation. The other scenario is during interaction between the coarsening precipitates and dislocations. "In hardened aluminium alloys, the dramatic increase of the temperature in the weld nugget has effect on both the solubility of Mg and Si and the atomic mobility. The solubility of Mg and Si increases in the Al matrix, and this leads to a high driving force for the decomposition of β'' needle" [26]. This effect plays a crucial role in grain sizes and grain boundaries as well as the associated mechanical properties.

3.3. Mechanical Properties Analysis

3.3.1. Microhardness Analysis.

Figure 6 shows the results of the microhardness test carried out in the stabilized region of the weld. The microhardness profiling was conducted across the weld traverse at a depth of 1.5 mm from the weld top surface. The unaffected parent metal average Vickers microhardness values is ~99 HV.

The plot shows a hardness decrease towards the weld retreating side for lower rotational speeds. The most affected hardness values are approximately 6.6 to 11 mm from the weld center on both sides of the welds. The rotational speed of 1100-rpm_60 mm/min recorded the least hardness value of ~ 49 Hv in the HAZ/TMAZ interface. This 48 % degradation in hardness is mostly characterized in the TMAZ. This is attributed to a combination of high stresses and large strains resulting in the deformation of the grain structure, where re-crystallization did not take place, caused a coarse grain structure [27].

Figure 6 demonstrated the degradation in hardness values at the interface of the regions attributed to softening of the material. Employing the rotational speed of 700-rpm achieved the highest peak values with distinct hardness variations in the weld nugget, more-so, for the lower feed rates of 60 and 80 mm/min. This is attributed to higher than normal fast cooling rates and varying thermal cycles resulting in poor material flow. Increasing the feed rate to 100mm/min improved the hardness values uniformity, however, with a decrease noticeable in the weld nugget towards the retreating side. The decrease is possibly due to unimproved fast cooling rates. Further increasing the rotational speed to 900-rpm, results in more uniform hardness values in the weld nugget attributed to optimum heat energy and stable thermal cycle effecting good material flow and stabilized cooling rates. However, the hardness value seems to decrease and this can probably be attributed mainly to the coarsening and dissolution of strengthening precipitates induced by the thermal cycle at the lower feed rates of 60 and 80 mm/min.

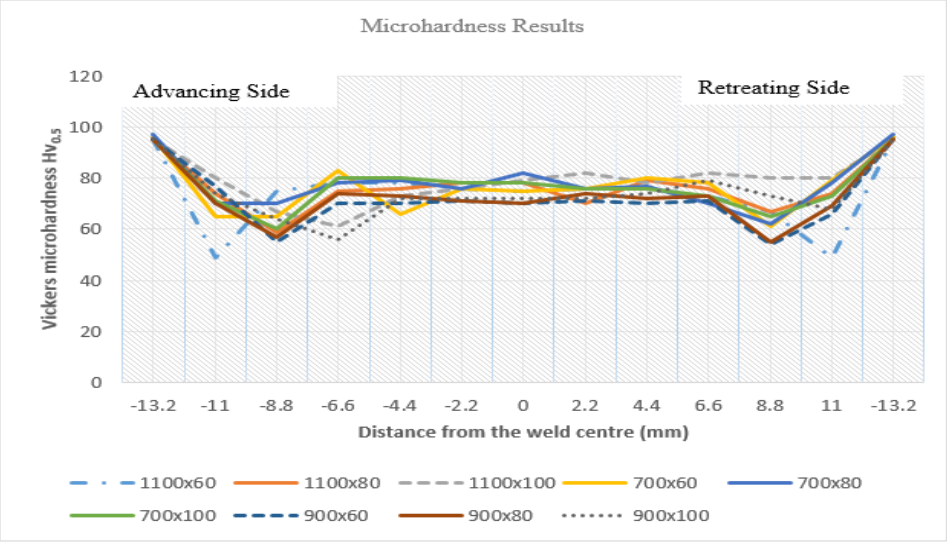

Fig. 6 Microharness values across weld traverse

Increasing the feed rates to 100mm/min, increased the hardness values which was a result of more plasticized material generated due to sufficient heat energy and permissible cooling rates. However, increasing the rotational speed to 1100 rpm at the lower feed rates improved the hardness in the weld nugget, however, with a decrease of hardness in the HAZ/TMAZ interface due to softening of the material. Further maintaining the rotational speed at 1100 rpm and increasing the feed rate to 100mm/min, shows a steep increase in the hardness values toward the retreating side, ranging from 67Hv in the HAZ/TMAZ advanced interface to 80Hv in the retreating HAZ side. This could be an effect of excessive plasticized material.

3.3.2. Mechanical Strength Analysis

The stress-strain behavior was studied and compared against each weld matrix as shown in Figure 7.

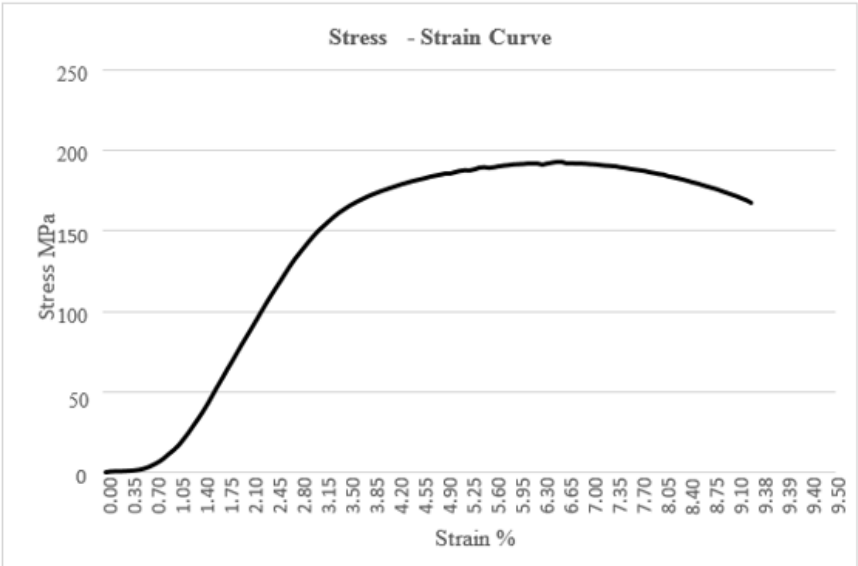

Fig. 7 Typical Stress-strain curve obtained from tensile test results of the weld sample for the process parameter 1100 rpm and 100 mm/min.

The weld sample processed using the combination of 900 rpm and 100mm/min gave the highest extension value of 4.225mm, and had the second highest ultimate tensile strength value of 191MPa (Table 6) and achieving the highest elongation. The parent metal's ductility, yield strength and ultimate tensile strength were 15%, ~271 and ~300 MPa respectively. Chen et al., reported the AA6061-T6 base metal elongation, yield strength and ultimate tensile strength of 12.1%, 242 MPa and 272 MPa respectively.

Table 6 demonstrates that all the weld samples exhibited reduction in the ultimate tensile strength and yield strength by between 34.8± 7% compared to the parent metal. The parent metal of AA6061-T6 is a hardened alloy which relies on precipitates. The thermal gradients and mechanical workings of the pin generated during FSW processing causes dissolution of the precipitates. This decomposition of precipitates and softened material gives rise to the reduction of the mechanical properties such as UTS and yield strength when compared with the base. The reduction of tensile strength inadvertently affects ductility.

As tabulated in Table 6, the FSW sample processed with the tool rotational and weld speeds of 1100rpm and 100mm/min respectively, recorded the maximum tensile strength, yield strength and weld efficiency of 192.51 MPa, 149.51 and 64.2% respectively. The variation of the ultimate tensile strength, yield strength and efficiency was within close range of between 181.73-192.51 MPa, 116.79-149.51 MPa, 60.5 % - 64.2%, respectively, for all the welded samples. It is also distinctively clear that for all the different tool rotation speeds, the ultimate tensile strength, yield strength and weld efficiency improved with increase in the weld speeds. It can be observed that all weld achieved their maximum UTS (192.51MPa, 191.17MPa, 189.94MPa) at the highest combinations of rotational and weld speeds. This could be attributed to the precipitates size and distribution improvement relative to optimum heat generation, which results in increase in mechanical properties relative to the increase in weld speeds. It can be noticed that a decrease in ultimate tensile strength is also uniform with the decrease in the yield strength and is relative to the decrease of the rotational and weld speeds.

Table 6 Mechanical Properties - Tensile Strength Values

Sample	Rotational Speed (rpm)	Welding Speed (rpm)	UTS (MPa)	Yield Strength (MPa)	η comparison to BM
BW1	700	60	183.63	114.26	61.2
BW2	700	80	186.57	147.88	62.2
BW3	700	100	189.45	127.24	63.3
BW4	900	60	181.73	116.79	60.5
BW5	900	80	189.45	145.37	63.2
BW6	900	100	191.17	122.46	63.7
BW7	1100	60	184.49	113.76	61.5
BW8	1100	80	188.65	134.08	62.9
BW9	1100	100	192.51	149.51	64.2

4. Conclusion

- X-ray radiography imaging was successfully used to demonstrate that FSW achieved full weld penetration.

- The X-ray images also enabled conclusion that no root defects were observed on all the welds, also confirming full weld penetration, as evidenced by the microstructural analysis and mechanical properties evaluations.
- Selection of suitable process speeds helped to achieve optimum generation of heat energy sufficient to plasticize the material. The correct process parameters thus contributed to improved material flow, a condition important for improving uniformity of microhardness across the weld traverse.
- Higher rotational speeds and higher feed rates resulted in increased hardness values, with the highest values recorded in the weld nugget and the least values recorded in the SZ/TMAZ interfaces. This was evidenced by a W-shaped hardness distribution data across the welds traverse in some of the welds.
- The base metal showed higher mechanical properties when compared to all the weld regions. The degradation in tensile strength and ductility notable in the interfaces was commonly due to the precipitates decomposition caused by thermal variations from high heat inputs and mechanical workings.

Acknowledgements

The authors would like to acknowledge the University of Johannesburg, South Africa, for allowing us to use their facility to conduct the experimental investigation and acknowledgements extended to Professor Kailas Satish of Indian Institute of Science, Bangalore, India for producing the welds.

Reference

[1] W. Thomas, "Friction Stir Welding". UK Patent 5,460,317, 6 December 1991.

[2] W. Arbergast and P. Hartlet, "Friction stir welding technology development," in *Lockheed Martin Michoud Space system*, Georgia, US, 1998.

[3] E. Akinlabi, R. Mahamood and S. Akinlabi, "Processing Parameters Influence on Wear Resistance Behaviour," *Advances in Material Science and Engineering*, vol. 2014, no. Article ID 724590, pp. 1-2, 2014.

[4] M. Patil, "MTech Dissertation on study of effect of process parameters in friction stir welding of 5083 Al alloy on power input and microhardness contours in weld cross - sections," Indian Institute of Technology, Kharagpur, 2012.

[5] N. Khan, A. Siddiquee and S. Shihab, "Investigations on tunneling and kissing bond defects in FSW joints for dissimilar aluminium," *Alloys and Compunds*, vol. 648, pp. 360-367, November 2015.

[6] P. Kah, R. Rajan, K. Martkainen and R. Suoranta, "Investigation of weld defects in friction stir welding and fusion welding of aluminium alloys," *International Journal of Mechanical and Materials Science*, vol. 4, no. ISSN:1823-0334, December 2016.

[7] H. Chena, K. Yanb, L. Tao, S. Chena, C. Jiangb and Y. Zhaob, "The investigation of typical welding defects for 5456 aluminium alloy friction stir welds," *Elsivier Material Science and Engineering*, vol. 433, no. 1-2, p. October 2006, 64-69.

[8] M. Kathrotiya and K. Bhavsar, "Various Parameter Effects of Friction Stir welds," *International Research Journal of Engineering and Technology*, vol. 04, no. 02, February 2017.

[9] C. Devanathan and S. Babu, "Effect of plunge depth on Friction Stir Welding of Al 6063," in *2nd International Conference*, INCAMA, 2013.

[10] S. Bayazida and H. Farhangia, "Effect of Pin profile of depth of defects of Friction Stir welded 7075 Aluminium Alloy," *Elsevier Material Science*, vol. 11, pp. 12-26, 2015.

[11] C. Brook and C. Hanstead, "Impact of Non Destructive Testing," in *Proceeding on the 28th Annual British Conference of NDT*, Bristol, UK, September 1989.

[12] K. Oyindamola, "Master's Dissertation on Effects of Multi-Pass Friction Stir Processing on Aluminium," University of Johannesburg, Johannesburg, SA, 2016.

[13] C. Meola, A. Squillace, F. Memola, C. Minutolo and R. Morace, "Analysis of stainless steel welded joints: a comparison between destructive and non-destructive techniques," *Elsevier Material Processing Technology*, Vols. 155-156, pp. 1893-1899, 2004.

[14] T. Savaranana, B. Lahirial, V. Pillaib, J. Philip, B. Rao and T. Jayakumar, "Non-Destructive Evaluation of Friction Stir Welded Joints by X-Ray Radiography and Infrared Thermography," in *International Conference on Structural Integrity*, 2014.

[15] N. Gaurav, K. Manu and M. Sivashanmugam, "Digital Radiography Testing for GTAW and FSW Weldments on AA7075-T651 Aluminium Alloy," *Research india publications International Journal of Advanced Mechanical Engineering*, vol. 04, no. 7, pp. 747-754, 2014.

[16] P. Edwards and M. Ramulub, "Material Flow during friction stir welding of Ti-6Al-4V," *Elsevier Science Inc Journal of Materials Processing Technology*, vol. 218, pp. 107-115, April 2015.

[17] C. Patil, H. Patil and P. H, "Investigation on Weld Defects in Similar and Dissimilar Friction Stir Welded joints of Aluminium Alloys of AA7075 and AA6061 by X-ray Radiography," *American Journal of Material Engineering and Technology*, vol. 4, no. 1, pp. 11-15, 2016.

[18] B. Singh, "A handbook on Friction Stir Welding," in *978-3-659-10762-7*, UK, LAP Lambert Academic Publishing, June 2012, pp. 44-54.

[19] B. Kumar, V. Umapathi and J. Kumar, "A comparative study of mechanical properties and microstructures of FSW joints in Conventional welding joints," *Internation Journal of Engineering Trends and Technology*, vol. 35, 2016.

[20] P. Mashinini, "MTech Dissertation in Process window for Friction Stir Welding of 3 mm Titanium (Ti-6Al-4V)," Nelson mandela Metropolitan University, South Africa, May 2010.

[21] Z. Georgeou, "ME dissertation in the Analysis of Material Flow around retractable pin in FSW," Port Elizabeth Technikon, Port Elizabeth, South Africa, 2003.

[22] M. Lin, J. Shude, M. Xiangchen, Z. Yaming and G. Shuangsheng, "New technique for eliminating keyhole by active-passive filling friction stir repairing," *Researchgate Materials & design 97*, February 2016.

[23] F. Fadaeifard, K. Matori, S. Aziz, L. Zolkarnain and M. B. A. Rahim, "Effect of the Welding Speed on the Macrostructure Microstructure and Mechanical Properties of AA6061-T6 Friction Stir Butt Welds," *MDPI Journal of Metals*, vol. 7, no. 48, pp. 2-16, 2017.

[24] A. Sedmak, R. Kumar, S. Chattopadhyaya, S. Hloch, S. Tadic´, A. Djurdjevic´, I. C˘ ekovic´ and E. Donc˘eva, "Heat input effect of friction stir welding on aluminum alloy AA 6061-T6 welded joint," *Thermal Sciences*, vol. 20, p. 637–641, 2016.

[25] E. Akinlabi, "Doctoral Thesis on Characterisation of dissimilar Friction Stir Welds Between 5754 Aluminium Alloy and C11000 Copper," Nelson Mandela Metropolitan University, Port Elizabeth, South Africa, December 2010.

[26] X. Sauvage, A. Dédé, A. C. Muñoz and B. Huneau, "Precipitate stability and recrystallisation in the weld nuggets of friction stir welded Al-Mg-Si and Al-Mg-Sc alloys.," *Elsvier Science Inc Material Science Engineering*, vol. 491, pp. 364-371, 2008.

[27] Z. Chen, S. Li and L. Hihara, "Microstructure, mechanical properties and corrosion of friction stir welded 6061 Aluminum Alloy," in *University of Hawaii*, Manoa, Honolulu, HI 96822, USA.

[28] P. Kah, B. Mvola, J. Martikainen and R. Suoranta, "Real Time non destructive testing of welding," *Trans Tech Publications Advanced Material Research,* vol. 933, no. 01, pp. 109-116, 2013.

[29] *Standard: ASTM B308/B308M Specification for Aluminium Alloy 6061-T6 Standard Structural profiles,* October 2010.

[30] *Standard Test Methods for Microidentation hardness of material ASTM384-16,* West Conshohocken, PA: ASTM International, 2012.

[31] *Standard Test Methods for tension Testing Wrought and Cast, ASTM B557-14,* 2014: ASTM International, West Conshokocken, PA.

[32] *Standard Test Method for tension testing of Mettalic Material,* West Conshohocken, PA: ASTM Test Methods , 2013.

[33] *Standard Reference Radiographs for Inspection of Aluminium and Magnesium Castings, ASTM E155-15,* West Conshohocken, PA: ASTM International, 2015.

[34] Z. Chen, S. Li and S. Hihara, "Microstructure, mechanical properties and corrosion of friction stir welded 6061 Aluminum Alloy," Hawaii Corrosion Laboratory Department of Mechanical Engineering University of Hawaii, Manoa, Honolulu, HI 96822, USA.

[35] "Wikipedia," Friction Stir Welding, [Online]. Available: https:/en.wikipedia.org/wiki/Friction_stir_welding.

[36] C. Brook and C. Hanstead, "Impact of Non DestructiveTesting," in *Proceeding on the 28th Annual British Conference of NDT,* Bristol, UK, September 1989.

[37] P. Kah, B. Mvola, J. Martikainen and R. Suoranta, "Real Time non destructive testing of welding," *Trans Tech Publications Advanced Material Research,* vol. 933, no. 01, pp. 109-116, 2013.

[38] C. Bird, "Ultrasonic phased array inspection technology for the evaluation of friction stir welds," *The British Institute of non-Destructive testing and Condition Monitoring,* vol. 46, no. 1, pp. 31-36, 1 January 2004.

[39] C. Meola, A. Squillace, F. Memola, C. Minutolo and R. Morace, "Analysis of stainless steel welded joints: a comparison between destructive and non- destructive rechniques," *Elsevier Material Processing Technology,* vol. 155, no. 156, pp. 1893-1899, 2004.

[40] "The Welding Institute," [Online]. Available: http:/www.twi-global.com/technical-technology/job-konwledge/non-destructive-examination-nde-part-1-liquid-penentrant-and-magnetic-particle-inspection-122.

[41] C. Bird, "Ultrasonic phased array inspection technology for the evaluation of friction stir welds," *The British Institute of Non-Destructive Testing and Condition Monitoring,* vol. 46, no. 1, pp. 31-36, 1 January 2004.